Available online at www.sciencedirect.com

ScienceDirect

Physics Procedia 83 (2016) 825 – 832

Physics Procedia

9th International Conference on Photonic Technologies - LANE 2016

Experimental study of residual stresses in metal parts obtained by selective laser melting

C.E. Protasov[a], V.A. Safronov[a], D.V. Kotoban[a], A.V. Gusarov[a,b,]*

[a]*Moscow State University of Technology "STANKIN", Vadkovsky per. 3a, 127055 Moscow, Russia*
[b]*Institute of Photonic Technologies (LPT),Friedrich-Alexander-Universität Erlangen-Nürnberg, Konrad-Zuse-Str.3-5, 91052 Erlangen, Germany*

Abstract

High local temperature gradients occur at additive manufacturing by selective laser melting of powder. This gives rise to undesirable residual stresses, deformations, and cracks. To understand how to control the formation of the residual stresses, a reliable method is necessary for measuring their distribution in the fabricated part. It is proposed to cut the part into thin plates and to reconstruct the residual stresses from the measured deformation of the plates. This method is tested on beams with square cross-section built from stainless steel. The beams were cut by electrical discharge machining and chemically etched. The obtained stress profile in vertical transversal direction slightly increases from the top to the bottom of the beam. This dependency is confirmed by numerical modeling. The measured stress profile agrees with the known results by other authors.

Peer-review under responsibility of the Bayerisches Laserzentrum GmbH

Keywords: electrical discharge machining; chemical etching; elastic modulus; yield strength

1. Introduction

Selective laser melting (SLM) is a layer-by-layer additive manufacturing technique where parts are built from powder. A thin powder layer is mechanically deposited on the growing surface and then selectively bound by a scanning laser beam. The powder and the underlying material are melted in the laser-interaction zone. The quality of the obtained material is comparable to that attained in metallurgical processes. An important and well-known drawback of SLM is the formation of high residual stresses and deformations, which may be responsible for

* Corresponding author. Tel.: +49-9131-85-23241 .
E-mail address: av.goussarov@gmail.com

Peer-review under responsibility of the Bayerisches Laserzentrum GmbH
doi:10.1016/j.phpro.2016.08.085

cracking and distortion of the built part. This problem is common for other laser technologies like welding because the laser beam heats a local zone to a high temperature while the rest of the part remains at the ambient temperature. Thus, a strong thermal shock is generated.

Gusarov et al. (2011,2013) showed that the conventional thermoelastic model is applicable to estimate residual stresses at SLM of several polymers and ceramics. In the framework of this model, the distribution of residual stresses is independent of the complicated transient temperature field in the part during the process. It depends on the shape of the zone where the temperature has attained the melting (softening) point where the thermal stresses are relaxed completely. The model is simple, so that the results are easy to analyze. For example, the residual stresses are proportional to the difference between the melting temperature and the ambient one. This is in line with the experimentally verified method of preheating, see Deckers et al. (2014).

Thermoplastic deformation of metal alloys is important under typical SLM conditions. In this case, the thermoelastic model may show qualitative tendencies, but rigorous calculation of the residual stresses requires a more complicated thermomechanical model. Thus, Brückner et al. (2007) and Zaeh and Branner (2010) used the model of elastoplastic flow combined with transient heat transfer. This numerical approach is time consuming because of two different scales in the problem, namely the size of the part and that of the laser-interaction zone. The existing numerical methods can estimate the distribution of residual stresses in metal parts. However, a deep parametric analysis is necessary for optimizing the process.

Various approaches to experimental measurement of residual stresses at SLM are being developed. Zaeh and Branner (2010) applied neutron diffraction and Yadroitsev and Yadroitsava (2015) used X-ray diffraction. In the diffraction methods, the sampling area is generally determined by the beam diameter while fine focusing may be difficult. Moreover, the penetration depth of the rays into the studied material cannot be changed. Thus, additional efforts are often necessary for positioning the sampling zone in depth. Therefore, the spatial resolution of the diffraction methods may be insufficient for small parts with nonuniform stress distribution.

Another group of experimental methods is based on deformation analysis at cutting the part. Wire electric discharge machining (EDM) is used because of its small influence zone. Zaeh and Branner (2010) studied deformation of SLM-fabricated t-shaped cantilever after cutting the supports. Mercelis and Kruth (2006) applied crack compliance method to measure transversal profile of residual stress in beams fabricated by SLM. In this method, strain is measured during transversal cutting of the beam by wire EDM. The obtained data require mathematical treatment to derive the stress profile.

The objective of this work is to test another deformation analysis-based method for measuring the residual stresses of SLM. Longitudinal cutting of the beam is applied. This may increase the sensitivity because of a high length-to-width ratio of the beam. The mathematical treatment becomes more straightforward.

2. Methods and materials

Consider a beam with arbitrary transversal profile of normal longitudinal stress $\sigma(z)$ shown in Fig 1a. Let the cross-section of the beam in plane (YZ) be rectangular and the stress do not depend on Y-coordinate. Figure 1b shows a thin layer cut from the beam between transversal coordinates $z - h/2$ and $z + h/2$. The cutting changes the force balance. Therefore, the layer can elongate/contract and bend. If the beam is uniform along axis X, the relative longitudinal deformation is independent of x and determined by relative deformation ε_0 of the middle plane $z = z_0$ and curvature radius R as follows:

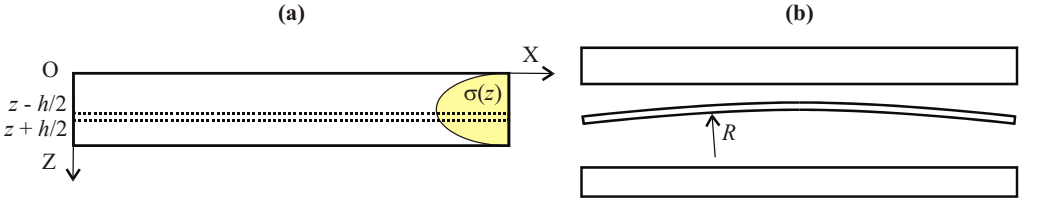

Fig. 1. Beam with residual stresses: (a) as fabricated; (b) after cutting a thin longitudinal layer.

$$\varepsilon = \varepsilon_0 + \frac{z_0 - z}{R}. \quad (1)$$

Suppose that the deformation of the thin layer is elastic. According to Hooke's law, the new stress distribution is

$$\sigma' = \sigma + \varepsilon E, \quad (2)$$

where E is the elastic modulus. Parameters ε_0 and R can be found from force and torque balances

$$\int_{z_0-h/2}^{z_0+h/2} \sigma' \begin{pmatrix} 1 \\ z \end{pmatrix} \mathrm{d}z = 0. \quad (3)$$

In the thin layer, the stress profile can be expanded in Taylor series as

$$\sigma(z) = \sigma(z_0) + (z - z_0)\frac{\mathrm{d}\sigma}{\mathrm{d}z}. \quad (4)$$

Equations (1)-(4) result in the following formulas for the stress σ and its z-derivative at the layer middle plane $z = z_0$:

$$\sigma = -\varepsilon_0 E, \quad (5)$$

$$\frac{\mathrm{d}\sigma}{\mathrm{d}z} = \frac{E}{R}. \quad (6)$$

Equation (5) is not useful to estimate the stress because the value of ε_0 is practically impossible to measure. However, Eq. (6) relates the derivative with the easily measurable curvature radius.

Note that Eq. (6) does not depend on the layer thickness. However, when the thickness increases, the precision of Taylor expansion by Eq. (4) decreases. Moreover, deformation due to bending increases with the distance from the middle plane according to Eq. (1). This means that deformations at cutting a thick layer from the sample can become non-elastic and violate Hooke's law by Eq. (2). Therefore, the layer should be as thin as possible to reduce the uncertainties. If the sample is cut into a set of thin layers, Eq. (6) can be integrated over z to obtain stress profile $\sigma(z)$. The integration introduces an unknown constant, which cannot be obtained in the framework of this method. However, the constant can be estimated from a known boundary value of σ.

Machine EOSINT M 280 was used to build beams from pre-alloyed stainless steel grade EOS PH1 fine powder produced by EOS Finland Electro Optical Systems Finland Oy. The chemical composition of stainless steel EOS PH1 reported by EOS (2016) is specified in Table 1. It corresponds to compositions DIN 1.4540 and UNS S15500. The manufacturer declares that 90% of powder volume constitute particles with size from 20 to 40 μm. Our granulometric analysis indicates that the average size of powder particles is d_m=26.12 μm, median size is d_{50}=26.08 μm, and the amount of powder particles with the size greater than 40 μm does not exceed 1.78%. As shown in Fig. 2, the beams were fabricated on a substrate. The substrate material is stainless steel AISI 321. The applied process parameters are recommended by Bandyopadhyay (2013) and are listed in Table 2. The estimated mechanical properties of the material obtained by SLM are presented in Table 3 according to EOS (2016).

Three beams were fabricated. Each beam was cut into seven plates of h = 1 mm thickness with wire EDM machine SEIBU M500 SG. Cutting width $a = D + 2\delta$ comprises wire diameter D = 0.2 mm and inter-electrode gap δ = 0.09 mm (see Fig. 2). According to Mercelis and Kruth (2006), EDM cutting introduces strong tensile stresses into the depth of about 40 μm from the cut surface. To exclude the influence of the cutting on the residual stresses formed at SLM, the top layer was removed by etching the plates in hydrochloric acid. The deformation of the plates was measured with coordinate machine WerhScopeCheck 200 using a contactless focus-variation sensor. Figure 3

shows the deformation of three plates measured at three points, at the ends and in the middle. The plates are cut from the three beams at the same distance from their top surfaces. The vertical displacement Δz is given relative the line connecting the ends. The parabolic approximation shown in Fig. 3 gives curvature radius R.

Table 1. Chemical composition of stainless steel EOS PH1.

Element	Fe	Cr	Ni	Cu	Mn	Si	Mo	Nb	C
Weight percent	Balance	14-15.5	3.5-5.5	2.5-4.5	Max. 1	Max. 1	Max. 0.5	0.15-0.45	Max. 0.07

Table 2. Process parameters.

Parameter	Value
Laser power (W)	195
Wavelength (μm)	1.06÷1.07
Beam offset (μm)	60
Height of layer (μm)	20
Scan speed (mm/s)	800
Hatching distance (mm)	0.1
Overlap (mm)	0.05

Table 3. Mechanical properties of laser-melted PH1.

Parameter	Value
Ultimate tensile strength, σ_u (MPa):	
- in horizontal direction (X and Y)	1200±50
- in vertical direction (Z)	1200±50
Yield strength, $\sigma_{0.2}$ (MPa):	
- in horizontal direction (X and Y)	1025±75
- in vertical direction (Z)	940±75
Elastic modulus, E (GPa)	200

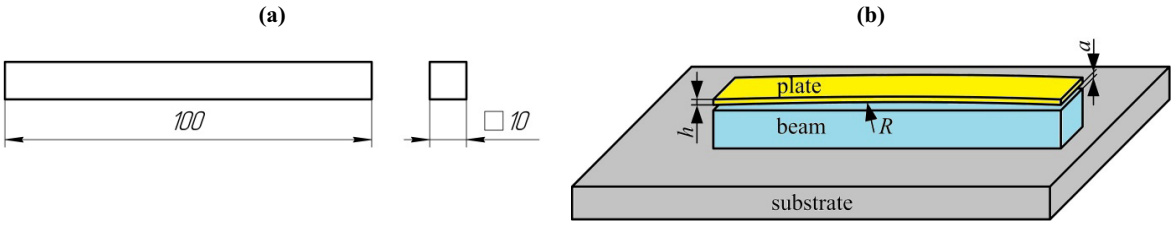

Fig. 2. Sample for studying residual stresses at SLM: (a) drawing of the beam; (b) beam on the substrate with the detached top plate. h is the plate thickness and a is the cutting width.

3. Results

All the obtained plates are convex from the top (see an example in Fig. 4a). The cross-section observed by optical microscope is shown in Fig. 5. The material consists of well-bonded beads of remelted powder with the diameter of about 100 μm. In the cross section, the beads look like fish scales. Several residual pores are seen in the cross section. The diameter of the pores is less than 10 μm. The pores are well separated from each other. The residual porosity is small, so that no influence on the mechanical properties is expected. Figure 5b shows that the

fish-scale structure is not modified after EDM. Slight darkening within about 100 μm from the cut surface may indicate a heat-affected zone.

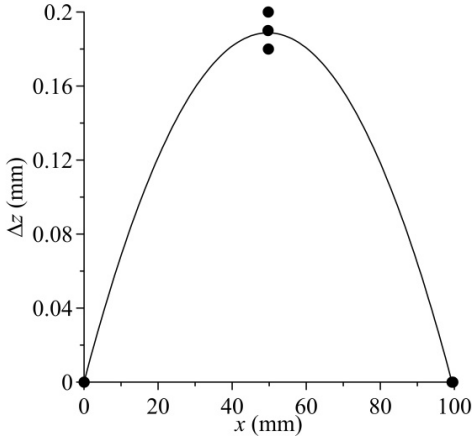

Fig. 3. Longitudinal profile of the vertical displacement measured at three points and the parabolic fit (curve).

Fig. 4. A plate before (a) and after (b) etching.

(a)

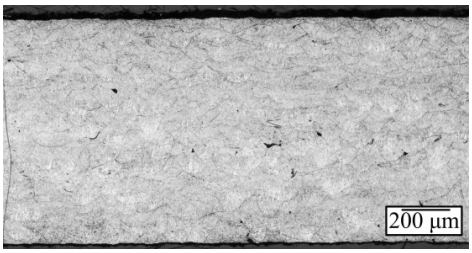

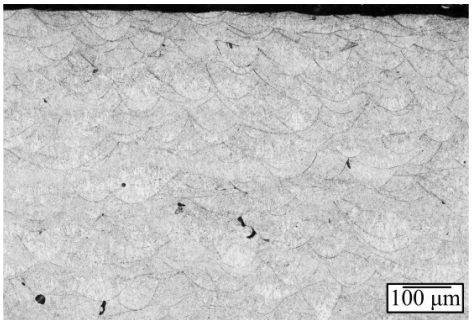

(b)

Fig. 5. Cross section of a plate after EDM: (a) general view; (b) near the top surface.

Deformation of several plates was measured during etching. The deformation is estimated by the vertical displacement of the middle point relative the line connecting the ends. It corresponds to the value of Δz at $x = 50$ mm in Fig. (3). The thickness of the plates during etching was measured at three points and averaged. The resulted plot of displacement versus the decrement of thickness is shown in Fig. 6. The sharp decrease of Δz in the decrement interval from 0 to 0.2 mm indicates that strong residual stresses are introduced by EDM within about 0.1 mm from each of two cut surfaces. Further etching does not significantly change the deformation. To eliminate the influence of EDM, all the plates were etched. The thickness before etching was 1 mm. The thickness after etching was from 0.4 to 0.6 mm. Thus, removing of a 0.2 mm layer from each cut surface is guaranteed.

Figure 7 shows curvature radius R of plates measured after etching versus distance z from the top of the bulk to the middle plane of the plate (see Fig. 1a). Every point indicates the average R of the three plates cut from the three beams at the same level z. The vertical bars indicate the standard deviation.

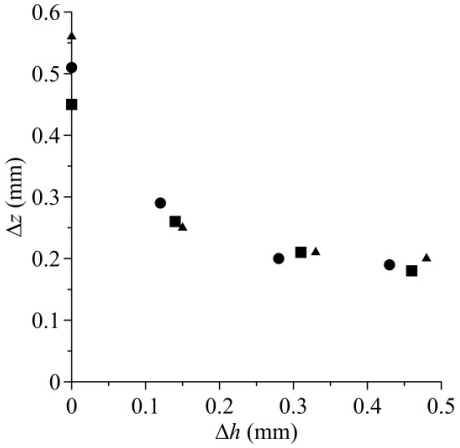

Fig. 6. Deformation z of plates at etching versus decrement of thickness b. Different symbols correspond to three different plates.

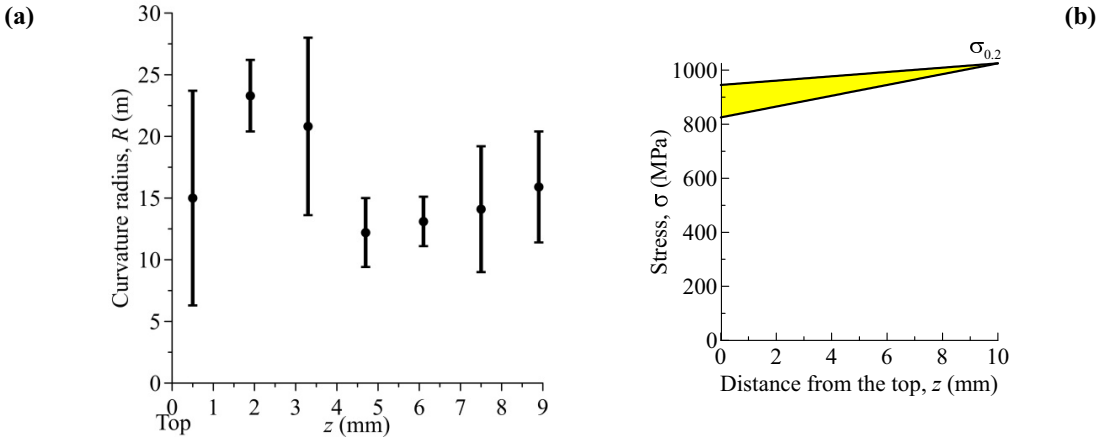

Fig. 7. (a) curvature radius R of a plate versus the distance from the top of the beam z; (b) reconstructed profile of residual stress σ.

4. Discussion

The uncertainty of the measured curvature radius is considerable, therefore no clear tendency for function $R(z)$ can be obtained from Fig. 7a. One can only conclude that the most of the values of R are in the range from 10 to 25 m. This value can be substituted into Eq. (6) along with the value of E from Table 3 to obtain that the gradient of the normal longitudinal stress $d\sigma/dz$ is in the range from 8 to 20 MPa/mm. Analysis of thermomechanical properties of metal alloys by Mercelis and Kruth (2006) and by Gusarov et al. (2013) indicates that shrinkage after laser melting is sufficient to attain plastic deformation. The first SLM layer is bonded to a massive substrate, which resists to shrinkage of this layer. Therefore, stress σ is likely to attain yield strength $\sigma_{0.2}$ = 1025 MPa (see Table 3) in this layer. In assumption that $\sigma = \sigma_{0.2}$ at the interface between the beam and the substrate, the estimated gradient value gives the stress profile shown in Fig. 7b.

Figure 7b indicates that stress σ slightly increases from the top to the bottom of the beam and its deviation from the yield strength $\sigma_{0.2}$ is less than 20%. Mercelis and Kruth (2006) suggested to apply condition $\sigma = \sigma_{0.2}$ on the top of the beam. In this case, Fig. 7b changes in a minor way and the above conclusion is still valid. A qualitative information about the stress distribution can be obtained using the thermoelastic mathematical model proposed by Gusarov et al. (2011,2013). The calculation result is shown in Fig. 8. Poisson's ratio is accepted to be 0.3. Other thermomechanical properties necessary for modeling are excluded by normalization proposed by Gusarov et al. (2013). The absolute values of σ are useless here because they should be considerably affected by plastic deformation. The calculated stress distribution is uniform in the middle of the beam between x = 30 mm and x = 70 mm. The top corners of the beam are unloaded. The unloading affects the end parts of the beam up to the distance of 2 to 3 beam height. These features follow from the geometry of the beam and should be common for the elastic medium and the elastoplastic one. The applied three-point method for measuring the curvature radius averages its value over the length of the beam. Therefore, the reconstructed stress profile shown in Fig. 7b also gives the stress averaged over the length. The unloading at the corners is likely to be responsible for the decrease of σ form the bottom to the top.

Depth profiles of the normal stress at SLM of steel 316L were recently measured by Yadroitsev and Yadroitsava (2015) by X-ray diffraction. They found that the stress fluctuates around a constant level without any tendency of increasing or decreasing with the depth. This level was also close to the yield strength. They used samples of 30x30 mm with height up to 1 mm. The diameter of the X-ray beam was about 1 mm. The stress was measured far from the periphery of the sample, so that the unloading could not influence their results. Thus, our results generally confirm those by Yadroitsev and Yadroitsava (2015). The small difference can be explained by the difference in the experimental conditions.

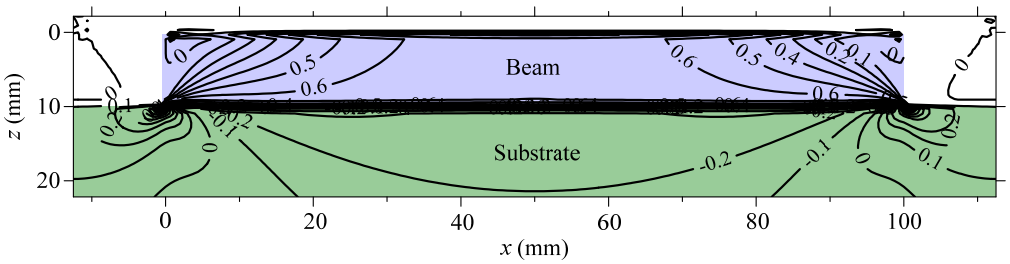

Fig. 8. Numerical modeling of the distribution of normal longitudinal stress σ in the longitudinal section of the beam on the substrate of the same material. The value of σ is normalized.

5. Conclusion

A method is proposed for experimental determination of residual stress distribution in a beam fabricated by SLM. It is based on cutting the sample into thin horizontal plates and measuring their curvature radii. The reconstructed stress distribution includes an unknown constant of integration, which should be estimated from a boundary value. Normal longitudinal stresses are measured in a beam from steel EOS PH1. The reconstructed stress slightly increases from the top to the bottom of the beam and its deviation from the yield strength is less than 20%. This dependence can be explained by unloading near the ends of the beam and is qualitatively confirmed by numerical modeling. The measured stress profile agrees with the known results of other authors.

Acknowledgements

This work has been financed by Russian Science Foundation (grant agreement No 15-19-00254 from 18.05.2015).

References

Bandyopadhyay, P.P., 2013. Influence of Sinking-in and Piling-up on the Mechanical Properties Determination by Indentation: A Case Study on Rolled and DMLS Stainless Steel. J. Materials Sci. Engineering A 576, 126.

Brückner, F., Lepski, D., Beyer, E., 2007. Modeling the influence of process parameters and additional heat sources on residual stresses in laser cladding. J. Thermal Spray Technology 16, 355.

Deckers, J., Meyers, S., Kruth, J.-P., Vleugels, J., 2014. Direct selective laser sintering/melting of high density alumina powder layers at elevated temperatures. Phys. Procedia 56, 117.

EOS, 2016. http://www.eos.info/.

Gusarov, A.V., Pavlov, M., Smurov, I., 2011. Residual stresses at laser surface remelting and additive manufacturing. Phys. Procedia 12, 248.

Gusarov, A.V., Malakhova-Ziablova, I.S., Pavlov, M.D., 2013. Thermoelastic residual stresses and deformations at laser treatment. Phys. Procedia 41, 889.

Mercelis, P., Kruth, J.-P., 2006. Residual stresses in selective laser sintering and selective laser melting. Rapid Prototyping J. 12, 254.

Yadroitsev, I., Yadroitsava, I., 2015. Evaluation of residual stress in stainless steel 316L and Ti6Al4V samples produced by selective laser melting. Virtual Physical Prototyping 10, 67.

Zaeh, M.F., Branner, G., 2010. Investigations on residual stresses and deformations in selective laser melting. Production Engineering 4, 35.